# Polar Direct Drive on the National Ignition Facility

**Introduction**

Recent advances in direct-drive target design have enhanced target performance beyond that achieved in the original baseline ignition design.[1] This substantially increases the probability of achieving moderate to high direct-drive target gain on the National Ignition Facility (NIF). The baseline direct-drive design for the NIF is itself very attractive. It achieves a target gain of 30 (70% of the 1-D gain) in 2-D simulations that include all expected sources of laser and target nonuniformity.[1] New developments have significantly enhanced direct-drive designs in three main areas (Fig. 96.7): (1) The fraction of laser light absorbed has been increased by almost 50% through the use of wetted-foam targets, providing increased energy coupling to the target.[2] This is the result of the higher-$Z$ material in the foam (e.g., carbon), which makes the plasma more collisional. (2) The hydrodynamic stability of the target has been significantly improved by adiabat shaping, which reduces the growth of target nonuniformities induced by the Rayleigh–Taylor instability without sacrificing target gain.[3] (3) Techniques using pulse shaping[4] and radiation preheat[5] have been developed to reduce the imprint of laser nonuniformities below that amount achieved by laser-beam smoothing alone. These enhancements allow the target to be driven to higher gain while improving hydrodynamic stability. Motivated by the enhanced performance predicted for direct-drive-ignition experiments on the NIF, this article examines the feasibility of employing direct drive, while the NIF is in the x-ray-drive configuration, as an additional approach to achieving ignition or near-ignition conditions. Polar direct drive (PDD) will couple more energy to the fuel than x-ray drive, and the compressed fuel core can be more easily accessed for high-$\rho R$ diagnostic development and fast-ignitor studies.

In the x-ray-drive configuration, the beams are clustered in the polar regions of the target chamber. To achieve the most-uniform target irradiation for direct drive, PDD repoints some of these beams toward the equator of the target (see **Beam-Pointing Strategy**, p. 213). Since these "equatorial" beams are more obliquely incident on the target than the remaining beams, they will have lower laser absorption and drive the target less efficiently. To compensate for the difference in polar and equatorial coupling, the laser intensity near the equator is increased relative to the pole, and different pulse shapes are employed to accommodate time-dependent variations in drive and absorption. The level of drive uniformity achieved by this technique is being studied using the 2-D hydrocode *DRACO*[6] (see **Two-Dimensional Simulation Results**, p. 215).

The target design used in these simulations employed both adiabat shaping and wetted foam (Fig. 96.7). Adiabat shaping is accomplished by means of an intensity picket imposed at the onset of laser irradiation. Because of its short duration, the shock launched by the picket is not fully supported, and it decays as it propagates through the target. This places the outer portion of the target shell, where the shock is strongest, on a high adiabat, and the inner portion of the shell, where the shock has weakened, on a low adiabat (adiabat is the ratio of the electron pressure to the Fermi-degenerate pressure). With proper choice of the picket intensity and duration, the high-adiabat region will be primarily confined to the ablation region of the target, leaving the main portion of the fuel on a low
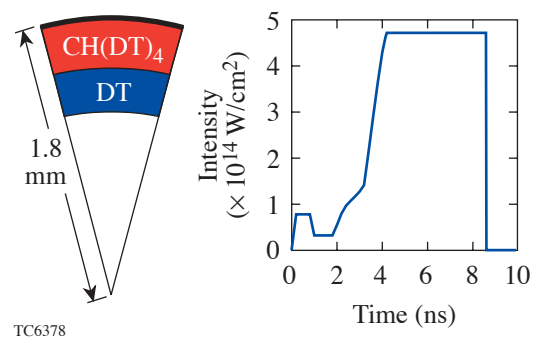


TC6378

Figure 96.7
Advanced direct-drive target designs employ wetted-foam targets for increased laser absorption and a picket at the beginning of the laser pulse to provide increased hydrodynamic stability. This target and pulse shape were used for the PDD simulations.

adiabat. The higher ablator adiabat produces higher ablation velocities and enhanced ablative stabilization of the Rayleigh–Taylor instability.[3] The lower adiabat of the main fuel layer allows greater compressibility of the fuel. The picket also reduces the amount of imprint on the target surface from laser nonuniformities.[4] Picket-fence pulses have been used previously as an alternative to continuous pulse shapes.[7] The picket used here has been specifically optimized for the purpose of shaping the adiabat in the fuel.

A comparison between the performance of wetted-foam designs with adiabat shaping and the performance of the baseline "all-DT" design was discussed in Ref. 2. The primary result was that wetted-foam designs achieved target gains typically two to three times higher than the gain for the all-DT target. The higher gain was the result of two factors: increased absorption and adiabat shaping. (1) Increased absorbed energy allowed more-massive targets to be driven with the same incident laser energy. (2) Adiabat shaping allowed the main portion of the fuel to be driven on a lower adiabat without compromising the shell integrity, resulting in higher areal density ($\rho R$). The stability of the wetted-foam target during the acceleration phase of the implosion was examined with 2-D simulations that calculated linear growth factors for different modes of nonuniformity.[8] The largest growth factor was 6.5 *e* foldings for a spherical-harmonic mode of 60, which is comparable to the stability obtained for the baseline x-ray-driven targets.[9]

It is not expected that polar-direct-drive targets will perform as well as "standard" direct-drive designs. In addition to the reduced laser coupling and the reduced hydrodynamic efficiency expected from the more-oblique irradiation near the equator of the target, there will be increased laser nonuniformity because the irradiation configuration has not been optimized for direct drive. For standard direct drive, the optimal irradiation distribution on target is known *a priori*; it must be uniform. For PDD, the irradiation pattern must be made intentionally nonuniform to compensate for the variations in target drive caused by variations in the laser angles of incidence around the target. As a result, PDD is a far more difficult design problem than standard direct drive. The required laser nonuniformity must be determined from computer simulations and confirmed by experiment.

**Beam-Pointing Strategy**

One possible irradiation strategy for PDD is to point the beams to the direct-drive positions on target, which are located along three latitudes at 23.5°, 44.5°, and 77.5° and correspond-

ing latitudes in the southern hemisphere.[10] (Here, the term *NIF beams* refers to the cluster of four beams that make up a "quad"; the term *ring of beams* refers to those beams that are pointed toward a particular latitude ring on the target and not to a ring of beam ports.) This beam pointing is illustrated in Fig. 96.8: The NIF x-ray-drive beam ports are shown as open circles, and arrows show the places on the initial target surface where each of the corresponding beams is pointed. When the NIF is converted to direct drive, the 30° beams will be relocated to the 77.5° ports (together with the 50° beams). For PDD, rather than pointing the 30° beams directly to the equatorial ring, a two-step procedure was used in order to minimize the angles of incidence near the equator. The four beams at 30° were pointed to direct-drive positions at 44.5°, and four of the eight beams that were already pointed to those positions were directed toward the 77.5° ring near the equator.



TC6149a

○ X-ray-drive port
● PDD pointing
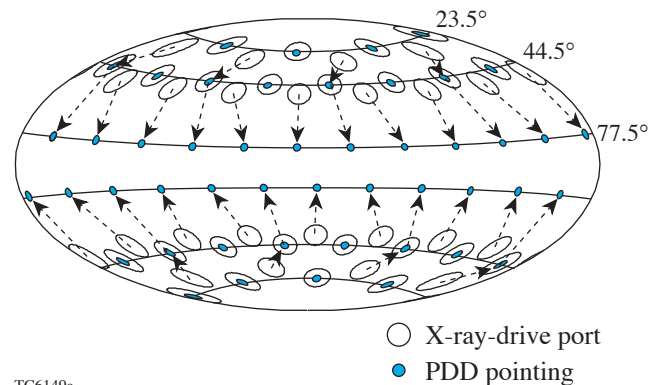
Figure 96.8
PDD repoints some beams from the NIF's x-ray-drive ports toward the target equator. This figure shows the beams being directed to the direct-drive positions corresponding to three rings of beams incident upon the target in each hemisphere.

Simply pointing the beams to the direct-drive positions does not, however, necessarily produce the optimal results for target drive uniformity. There are two main reasons: (1) Since the beam axes are not radially directed, their positions on the target surface will change as the target implodes; optimal uniformity at one time during the implosion may not be optimal at a later time. (2) The distribution of incident beam angles on target is not the same for the polar and equatorial regions; as a result, there will be variations in target drive due to spatial variations in laser absorption and in the density, where absorption occurs.

An example of the different angular distributions of incident rays is shown in Fig. 96.9 for two polar angles: 20° (characteristic of the polar region) and 90°. The normalized distribution of laser energy is plotted as a function of incident ray angle. This represents the simple projection of rays from the x-ray-drive ports onto a sphere, which is the initial size of the target. Each of the distributions has been averaged over all azimuthal angles and ±10° in the polar angle. The width of the distribution is the result of contributions from overlapping beams as well as the averaging. The distribution in the polar region is heavily weighted toward angles below 40° and is typical of the distribution around the target when beams originate from the direct-drive ports. The distribution of rays in the equatorial region is dominated by angles greater than 40°.
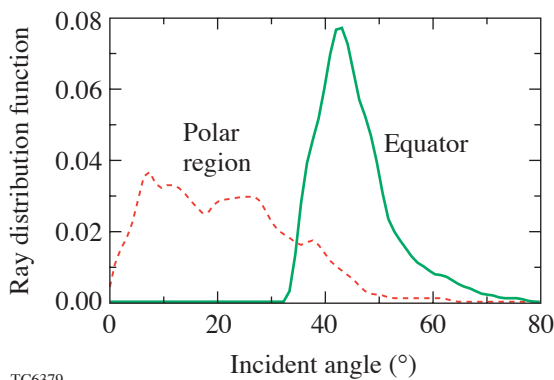


TC6379

Figure 96.9
The distribution of incident angles for the laser rays is calculated by projecting the beams from the NIF's x-ray-drive ports onto a sphere, using the beam pointing of Fig. 96.8. The distributions have been averaged over all azimuthal angles and ±10° in polar angle.

An indication of the variation in electron densities where the energy would be deposited is given by the turning points of the rays during refraction. Using a planar approximation, the electron density $n_e$ at the turning point of the rays is $n_e = n_c \cos^2\theta$, where $n_c$ is the critical density and $\theta$ is the incident angle of the rays. Thus, energy in the polar region is deposited typically above $0.6\,n_c$, and energy near the equator is deposited well below $0.6\,n_c$.

To improve the pointing strategy, absorption physics was added to the analysis. We used a target design (described in the following section) driven by uniform irradiation to obtain the density and temperature profiles at a time near peak laser irradiation. Rays were then tracked from the NIF x-ray-drive ports through the plasma atmosphere to calculate absorp-

tion as a function of the incident angle. The relative energy among the beams, the beam pointing, and the beam-spot shapes were varied to find the configuration that gave the lowest rms variation in absorption around the target. Optimal uniformity was found by pointing the beams to latitudes that were closer to the equator than the direct-drive positions in Fig. 96.8, namely 26°, 59°, and 82°. Elliptical spot shapes were used, with the ratio of major to minor axes being 1.0, 1.25, and 1.8, respectively.

Further optimization of the irradiation strategy must take into consideration the differences in hydrodynamic efficiency that result from variations around the target in density where the laser light is absorbed; time-dependent effects resulting from the target implosion and plasma evolution; and multidimensional effects such as lateral heat flow arising from temperature variations in the laser deposition region. The 2-D simulations include all these effects and were used as guidance on how to further improve the uniformity of target drive through the use of beam pointing, laser-focal-spot shapes, and pulse shapes.

**One-Dimensional Target Design Considerations**
One-dimensional simulations are useful to obtain insight into the sensitivity of target drive to the distribution of incident laser rays. They were used here to obtain a first estimate of the spatial variations in laser intensity that are required to compensate for the variations in incident laser light around the target. The results also identified a realistic target design for the 2-D simulations. These estimates neglect the effect of lateral mass and heat transport, which are included in the full 2-D simulation described in the next section.

A series of 1-D simulations were performed, each corresponding to a different latitude on the target. The distributions of incident laser rays for the different latitudes were estimated as done for Fig. 96.9. In each simulation, the target was uniformly irradiated with the distribution of rays corresponding to a particular latitude. The rays were traced in the spherical plasma profiles, but because of the spherical symmetry of the problem, only the radial location of the ray entered. The goal was to find a pulse shape corresponding to each latitude such that the resulting shock positions and shell positions were similar to those for the 20° latitude, within a few microns.

We used the $CH(DT)_4$, 1.5-MJ design (1.35 MJ absorbed) from Ref. 1 as the starting point. The design was further optimized for a target driven with the distribution of incident laser rays characteristic of the 20° latitude. This became the

baseline for determining pulse shapes at other latitudes. The 1-D simulations showed very little variation in the required pulse shapes for latitudes between 0° and 60°. However, to obtain similar target drive with the equatorial distribution of rays, the energy in the beams had to be increased by about 30%.

These 1-D estimates indicated that a 1.1-MJ target design should be used in the 2-D simulations: this should provide enough "headroom" to increase beam energies by 30% to 50%, if necessary, to compensate for the oblique irradiation near the equator. (This assumes a 1.6-MJ capability for the NIF.) The target and pulse shape were similar to the $CH(DT)_4$ design from Ref. 1, but they were scaled down for the incident energy of 1.1 MJ (see Fig. 96.7). The 1-D results were target gain = 54; absorbed energy = 1.0 MJ; peak implosion velocity = $4.1 \times 10^7$ cm/s; and peak $\rho R = 1.2$ g/cm$^2$. A stability analysis, using a postprocessor[11] to the 1-D code *LILAC*, showed that the mix region was only about 30% of the shell thickness during the acceleration phase of the implosion for this target.

This design was used as a baseline for the 2-D hydrodynamic simulations (see next section). In the 2-D simulations, the pulse shapes for the different rings of beams were adjusted to produce similar shock and shell conditions as achieved in the 1-D baseline simulation. Besides compensating for the reduced laser coupling at the equator, the pulse shapes had to compensate also for the lateral flow of deposited energy from the equator toward the pole. The 1-D estimates showed that coronal electron temperatures should be higher at the equator than in the nearby mid-latitude regions, due to the higher laser intensity required to drive that part of the target. This will result in lateral heat flow in the 2-D simulations.

**Two-Dimensional Simulation Results**

For the 2-D *DRACO* simulations, the NIF irradiation configuration was described in terms of the beams pointed to three latitude rings in each hemisphere, as shown in Fig. 96.8. The simulations discussed below used the latitudes 26°, 59°, and 82° relative to the initial radius of the target (see **Beam-Pointing Strategy**, p. 213). A ray-trace algorithm with refraction calculated the amount of laser absorption and the location of the deposited energy in the plasma atmosphere around the target. An azimuthal average of the deposition was used. Whereas a full three-dimensional ray-trace algorithm has been developed for PDD simulations in the Eulerian code *SAGE*,[12] an approximate treatment was implemented here for speed during optimization studies. The approximation used only the radial variation in the index of refraction to modify the ray trajectories and ignored lateral variations. An azimuthal aver-

age of the laser deposition determined how energy for each ring was distributed on the target. These simulations addressed only the gross nonuniformities in target drive that arise from beam placement and pointing. The effects of target-surface nonuniformities and beam nonuniformities will be examined in future work.

As the target implodes, the energy delivered to the equator changes relative to the pole because the beams are not pointed toward the target center. To compensate for the time-dependent effects, as well as 2-D effects resulting from lateral heat flow, different pulse shapes were used for the three rings of beams. A numerical algorithm was developed to automatically adjust pulse shapes during the simulation to compensate for nonuniform drive. Different tests were used to detect nonuniformities: During the time of shock propagation, variation in the mass-weighted, inward-moving velocity was used. After the time of shock breakout and during acceleration, variation in the outer position of the target shell (as defined by the location of the point at $1/e$ times peak density) was used. The pulse-shape-refinement algorithm adjusted the relative power among the pulses to increase laser deposition in regions where the target was moving too slowly and to decrease deposition in regions that were moving too rapidly. In practice the required variation in laser absorption around the target could be achieved only for long-wavelength nonuniformities because control is limited to only three degrees of freedom corresponding to the three rings of beams.

To adjust the pulse shape in each ring of beams, we calculated the energy deposition pattern for each ring separately on the target. The relative power in each ring was varied until the superposition of all the deposition patterns formed a best fit to the variation required to compensate for drive nonuniformities.

A technique known as proportional–integral–differential (PID) feedback, common in control theory,[13] was used to adjust the pulse shape for each ring of beams on the target. The source of the feedback was the spatial perturbation formed by sampling the nonuniformity during a *DRACO* simulation and then applying the proportional, integral, and differential feedback gain terms. The integral and differential terms act to dampen and stiffen the response function. A simple prescription to find the feedback gain terms can be found in Ref. 14. The Levenberg–Marquardt nonlinear optimization algorithm[15] was employed to find the optimal choice for the relative strengths among the rings of beams such that the combined absorption variation provides a best fit to the feedback perturbation. Spherical-harmonic modal space was used in lieu of physical

space in the algorithm because the Levenberg–Marquardt algorithm allows for the optimization of a predetermined set of modes. For instance, certain modes considered the most dangerous can be given a larger weight during optimization. Note that in the limit of zero feedback gain, the optimization procedure reduces to a minimization of the rms variation of absorbed energy.

The pulse-shape refinement algorithm was not able to respond adequately to nonuniformities that were highly localized around the equator. To compensate for the reduced energy deposition at the equator from the very oblique incident irradiation, it is necessary to substantially increase the relative amount of energy deposited in that region by the equatorial ring of beams. However, if the spot shape were made sufficiently elliptical to localize the energy to the equatorial region, its contribution to uniformity through beam overlap in the mid-latitudes would be reduced. The problem was addressed by using a beam profile that was parameterized as the superposition of two super-Gaussian profiles (illustrated in Fig. 96.10). The main part of the spot shape is a super-Gaussian profile that contributes to beam overlap in the mid-latitudes as well as the equator. Superimposed on this is a highly elliptical super-Gaussian profile that concentrates additional energy only in the equatorial region. The aspect ratio of the ellipse, its relative location, and its relative energy are adjustable parameters that were varied in a series of 2-D simulations to find the optimal drive uniformity. In the simulations below, the ratio of major to minor axes was 5; the center of the superimposed ellipse was offset from the main spot by 10% of the target radius in the direction of the equator; and its peak intensity was 20% of the peak intensity for the main spot. The shape of the main part of the beam was also varied, and a 1.8:1 ellipse was used in the simulations below.

The three pulse shapes generated by the pulse-shape refinement algorithm resulted in the intensity variations shown in Fig. 96.11(a) for the pole and equator. The intensity variation for all polar angles is shown in Fig. 96.11(b) for the times 4.2 ns and 8 ns. At 4.2 ns, the intensity variation is relatively flat, increasing by about 30% only near the equator. This is consistent with the 1-D estimates. At 8 ns, there is a dip in the incident intensity at 45°, followed by a factor-of-2 increase at the equator. This is a 2-D effect. The temperature at the equator becomes larger than in the mid-latitudes due to the increased intensity required to drive that portion of the target. Lateral heat flow moves some of the energy deposited at the equator toward the 45° latitude. Consequently, less laser light needs to be deposited at 45° to obtain the required target drive at that location, but more energy must be deposited at the equator.

The resulting drive uniformity was adequate to achieve a high value of fuel $\rho R$ during the implosion, but further improvements in uniformity are required to actually reach ignition. The PDD simulation tracked the corresponding 1-D result up to the onset of hot-spot formation. A comparison between the PDD angularly averaged density profile and the 1-D profile at the end of the acceleration phase of the implosion is shown in Fig. 96.12. At this time, the shell radius has converged by almost a factor of 4. The positions and magnitudes of the peaks are very similar; however, there were density variations of ±20%, pressure variations of ±10%, and a variation in the outer surface of the shell of ±5%. These nonuniformities continued to grow during the deceleration phase of the implosion.
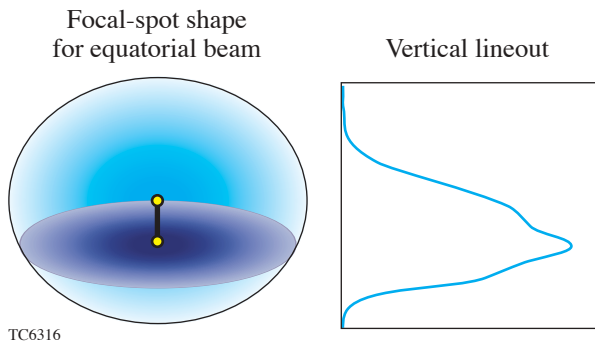


Figure 96.10
The spot shape for the equatorial ring of beams is chosen as the superposition of two super-Gaussian profiles. The larger profile contributes to irradiation uniformity at the mid-latitude regions, as well as near the equator. The highly elliptical profile concentrates additional energy very close to the equator.
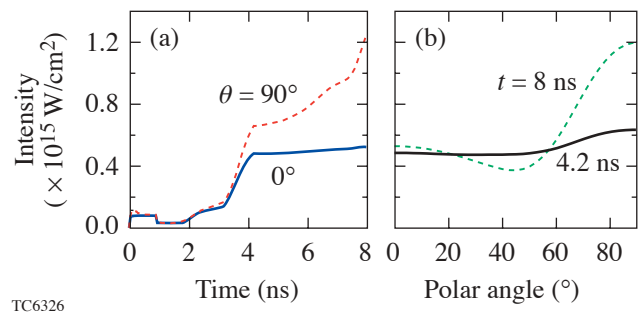


Figure 96.11
The variation in intensities at the pole and equator shows the compensation required for PDD: (a) the temporal variation in intensity at the pole and equator; (b) the angular variation in intensity at times 4.2 and 8.0 ns.

Near the time of hot-spot formation, when the shell had converged an additional factor of 6, the target nonuniformities had grown sufficiently large that the resultant shell distortion prevented further development toward ignition. A density contour plot at this time in the simulation is shown in Fig. 96.13, together with the temperature contours for 10, 8, 6, and 4 keV in the hot-spot region. High-density spikes are starting to penetrate into the hot region. In Fig. 96.14, the

angular average of both the temperature and density is compared with 1-D profiles as a function of $\rho R$. The temperature profiles are similar, with the hot region extending to a $\rho R$ of ~0.1 g/cm$^2$. Over the next 100 to 200 ps, the 1-D simulation extends the hot region to a $\rho R$ of 0.2 to 0.3 g/cm$^2$ and ignition occurs. The 2-D simulation failed to continue forming the hot spot beyond this point due to extensive growth of shell distortion. In Fig. 96.14, the contribution of shell distortion is evident in the width of the angularly averaged density profile.

Even though ignition did not occur in this simulation, the conditions achieved during the time of neutron production could be very useful for the development of high-$\rho R$ diagnostics and the investigation of fast-ignitor physics.[16] The neutron-averaged $\rho R$ was 1.1 g/cm$^2$, and the neutron yield was $6 \times 10^{16}$ (corresponding to a target gain of 0.1).

Strategies to improve the uniformity of target drive for PDD are being developed. The automated pulse-shape refinement algorithm is being further optimized to better detect drive nonuniformity and adjust pulse shapes accordingly. For a given set of beam-pointing and spot-shape conditions, it may not be possible to achieve adequate drive uniformity by adjusting the pulse shapes. Thus, the specifications for beam pointing and spot shapes are also being refined. Target "shimming," in which the target shell is made thinner at the equator than at the pole, is another technique that will be examined for improving drive uniformity. Conditions very close to ignition have been achieved here. An additional factor-of-2 improvement in drive uniformity will probably be adequate for the target to ignite.
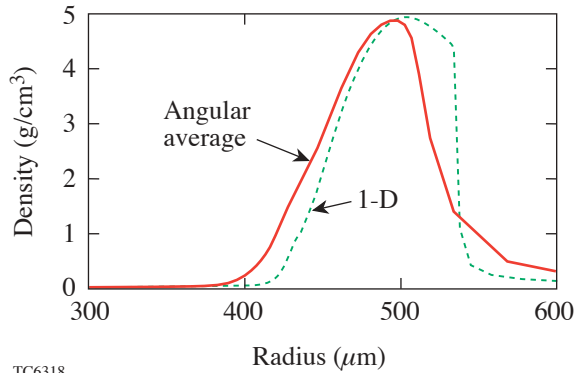


TC6318

Figure 96.12
The angular average of the density profile from the PDD simulation is compared with the corresponding 1-D density profile at the end of the acceleration phase of the implosion (8.2 ns).
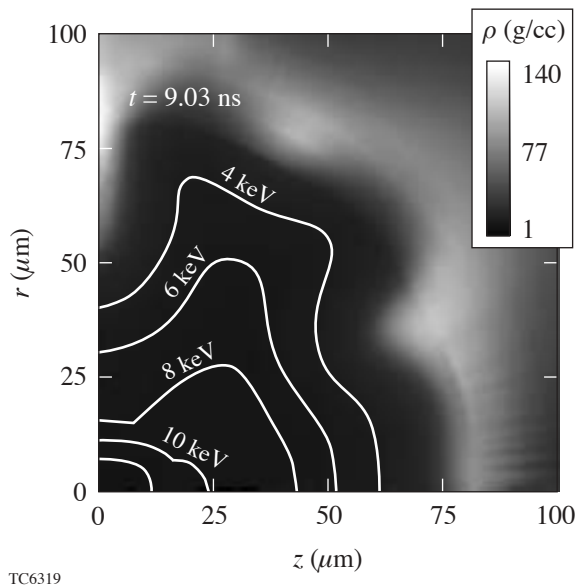


TC6319

Figure 96.13
Density contour plot at the onset of hot-spot formation (9.03 ns) shows spikes starting to penetrate the hot region. Temperature contours of 10, 8, 6, and 4 keV are shown.
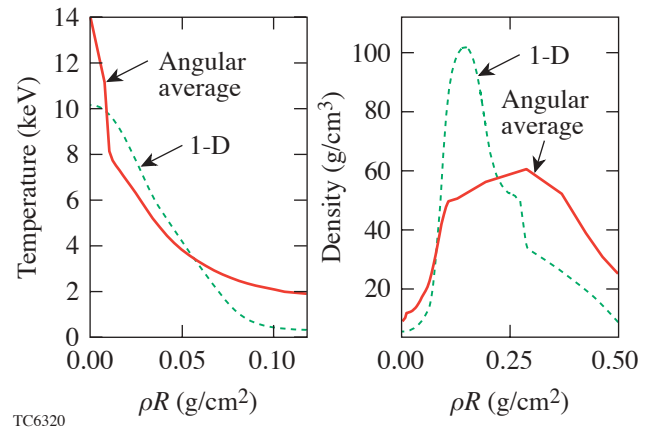


TC6320

Figure 96.14
The angular averages of temperature and density profiles from the PDD simulation near the onset of hot-spot formation (9.03 ns) are compared with the 1-D results.

The computer simulations used to identify optimal irradiation strategies will be validated by experiments on the OMEGA laser.

## PDD Experiments on OMEGA

Three sets of experiments planned for the OMEGA laser over the coming year are designed to validate the computer modeling of target performance driven by oblique irradiation. One set of experiments will investigate shock propagation in planar geometry using cryogenic $D_2$ and wetted-foam targets. The OMEGA beam geometry can irradiate a planar target with beams at 23°, 48°, and/or 60° angles of incidence. The main diagnostic will be the measurement of the time of shock breakout at the rear of the target.

The second set of experiments will irradiate spherical targets uniformly, but with all the beams repointed to make the beam axes equally oblique to the target surface. The symmetry of the OMEGA irradiation geometry can be maintained by repointing all beams by the same amount. This can be achieved as shown in Fig. 96.15: The beams of the OMEGA laser are configured as 12 pentagonal groups. The angle of incidence of each beam axis on the initial target surface can be changed from normal to 24.8° by pointing each beam to a place on the target that corresponds to the position of a neighboring beam in the pentagon. This tests the modeling of laser absorption and target drive with oblique irradiation, without introducing the complication of large variations in irradiation conditions around the target.
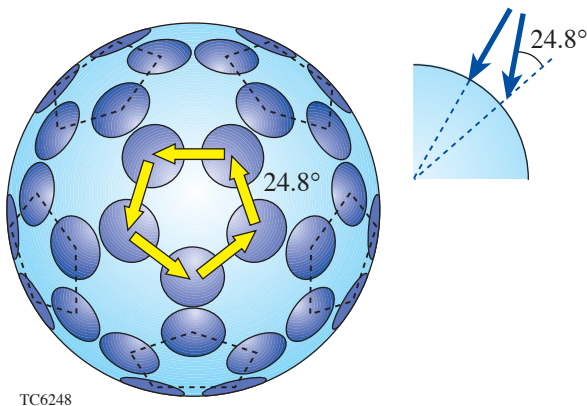


TC6248

Figure 96.15
One of the PDD experiments planned for the OMEGA laser will repoint all beams by the same amount to maintain irradiation uniformity while driving an implosion with oblique irradiation.

The third set of experiments will be a more direct characterization of PDD on the NIF. In this case, 40 of the 60 OMEGA beams will be used to populate only the beam ports near the polar regions, providing a good approximation to the polar-direct-drive conditions that will occur on the NIF. The beams will then be repointed, and the pulse shapes adjusted (within the limitations of OMEGA), to drive spherical implosions. These will be compared with 2-D simulations.

## Summary

The recent progress in direct-drive target design makes the direct-drive approach to inertial confinement fusion a very attractive candidate for achieving high gain on the NIF. Adiabat shaping is a very powerful technique to enhance target stability. When combined with the increased laser absorption possible in wetted-foam targets, 1-D target gains of the order of 80 are possible.

Direct-drive target physics can be examined while the NIF is in the x-ray-drive configuration by pointing some of the beams toward the target equator. This polar-direct-drive approach presents more-difficult design problems than standard direct drive, which uses a beam configuration already optimized for the required level of irradiation uniformity. For PDD, the incident irradiation must be made intentionally nonuniform—higher in the equatorial region than in the polar region—to accurately compensate for the spatial variations in laser absorption and hydrodynamic efficiency. Simulations have not yet demonstrated ignition with PDD, and the optimization process is still in progress. Nevertheless, high values of $\rho R$ and high neutron yield have been obtained in the simulations, suggesting that, at the very least, PDD can be an attractive technique for high-$\rho R$ diagnostic development and fast-ignitor experiments. PDD might be the best approach for fast-ignitor experiments while the NIF is in the x-ray-drive configuration because of the relatively large amount of energy that can be coupled to the fuel and because the ignitor beams can access the compressed core without passing through a hohlraum.

REFERENCES

1. P. W. McKenty, V. N. Goncharov, R. P. J. Town, S. Skupsky, R. Betti, and R. L. McCrory, Phys. Plasmas **8**, 2315 (2001).

2.  S. Skupsky, R. Betti, T. J. B. Collins, V. N. Goncharov, D. R. Harding, R. L. McCrory, P. W. McKenty, D. D. Meyerhofer, and R. P. J. Town, in *Inertial Fusion Sciences and Applications 2001*, edited by K. Tanaka, D. D. Meyerhofer, and J. Meyer-ter-Vehn (Elsevier, Paris, 2002), pp. 240–245.

3.  V. N. Goncharov, J. P. Knauer, P. W. McKenty, P. B. Radha, T. C. Sangster, S. Skupsky, R. Betti, R. L. McCrory, and D. D. Meyerhofer, Phys. Plasmas **10**, 1906 (2003).

4.  T. J. B. Collins and S. Skupsky, Phys. Plasmas **9**, 275 (2002).

5.  S. P. Obenschain *et al.*, Phys. Plasmas **9**, 2234 (2002).

6.  A short description of the hydrocode *DRACO* is contained in P. B. Radha, V. N. Goncharov, T. J. B. Collins, J. A. Delettrez, P. W. McKenty, and R. P. J. Town, "Two-Dimensional Simulations of Plastic-Shell Implosions on the OMEGA Laser," to be submitted to Physics of Plasmas.

7.  J. D. Lindl and W. C. Mead, Phys. Rev. Lett. **34**, 1273 (1975).

8.  T. J. B. Collins, S. Skupsky, V. N. Goncharov, R. Betti, P. W. McKenty, P. B. Radha, R. Epstein, A. Poludnenko, A. Frank, and S. Mitran, "High-Gain, Direct-Drive Foam Target Designs for the National Ignition Facility," to be published in *Inertial Fusion Sciences and Applications 2003* (Elsevier, Paris, 2004).

9.  M. C. Herrmann, M. Tabak, and J. D. Lindl, Phys. Plasmas **8**, 2296 (2001).

10. S. M. Pollaine and S. W. Haan, *ICF Quarterly Report* **8**, 15, Lawrence Livermore National Laboratory, Livermore, CA, UCRL-LR-105821-98-1 (1997).

11. V. N. Goncharov, P. McKenty, S. Skupsky, R. Betti, R. L. McCrory, and C. Cherfils-Clérouin, Phys. Plasmas **7**, 5118 (2000).

12. R. S. Craxton, Bull. Am. Phys. Soc. **48**, 56 (2003).

13. W. S. Levine, *The Control Handbook* (CRC Press, Boca Raton, FL, 1996).

14. See Ziegler–Nichols tuning rules, in K. Ogata, *Modern Control Engineering*, 3rd ed. (Prentice-Hall, New Jersey, 1997), Chap. 10, pp. 672–674.

15. W. H. Press, *Numerical Recipes in C: The Art of Scientific Computing* (Cambridge University Press, Cambridge, England, 1988), pp. 540–547.

16. M. Tabak *et al.*, Phys. Plasmas **1**, 1626 (1994).